Climate Dynamics (2000) 16:479–489 

B. Gallego · P. Cessi

# Exchange of heat and momentum between the atmosphere and the ocean: a minimal model of decadal oscillations

Received: 15 December 1998 / Accepted: 29 October 1999

**Abstract** A model of the large-scale interaction between the troposphere and the upper ocean, wind-driven circulation is formulated. Simplified parametrizations, built upon the conservation of global heat and momentum, relate the atmospheric eddy heat and momentum fluxes to the zonally averaged oceanic and atmospheric temperatures. The formulation shows that the wind-driven circulation influences the winds by controlling the strength of the oceanic northward heat transport, and thus the atmospheric northward heat transport and temperature distribution. Because the ocean takes decades to adjust to changes in the winds, the coupled system equilibrates into a state which is periodic in time, rather than steady. The period is linearly proportional to the transit time of long Rossby waves across the basin, and thus is of the order of decades for large-scale basins.

## 1 Introduction

Progressively longer oceanic and meteorological time series have not yet revealed spectral saturation at low-frequency: the ocean and atmosphere fluctuate on time scales as long as those resolved by the measurements. Specifically, the North Atlantic sea-surface and subsurface temperatures, sea-level pressure and surface winds all show variations in their large-scale patterns on interannual and interdecadal time scales (e.g., Deser and Blackmon 1993; Kushnir 1994; Plaut et al. 1995; Mann and Park 1996; Moron et al. 1998).

B. Gallego (✉)
Department of Atmospheric Sciences,
UCLA, 7127 Math Sciences Building, Los Angeles,
CA 90095-1565, USA
E-mail: blanca@atmos.ucla.edu

P. Cessi
Scripps Institution of Oceanography,
UCSD, La Jolla, CA, USA

The North Pacific also exhibits variability at the barely resolved decadal time scales (Trenberth and Hurrell 1994). The variance in sea-surface temperature (SST) on these time scales is concentrated near the two major mid-latitude oceanic fronts, and some of it appears to be of mid-latitude origin, uninfluenced by the tropics, where El Nino-Southern Oscillation dominates the interannual fluctuations (Nakamura et al. 1997).

Several mechanisms for such variability can be postulated: fluctuations in the oceanic variables can be forced by the variability of the atmospheric circulation (either intrinsic or anthropogenically induced); intrinsic ocean variability can force long-term fluctuations in the atmosphere; the combined ocean-atmosphere system has inherently coupled fluctuations. It is likely that all of these mechanisms play some role, but teasing them apart with the aid of observational data alone is a daunting task.

Studies using general circulation models (GCMs), aimed at elucidating the response of the midlatitude atmosphere to prescribed SST have given contradictory results (Kushnir and Held 1996), but some coupled GCMs suggest that large-scale variability at interdecadal time scales in the Northern Hemisphere basins may stem from an interaction between the atmosphere and the ocean (Latif and Barnett 1994, 1996; Grötzner et al. 1998). The interpretation offered by these authors is that coupled decadal variability might arise due to the difference in the adjustment times of the general circulation of the atmosphere and of the ocean. Specifically, the wind-driven oceanic circulation takes decades to equilibrate to changes in the winds, which in turn are affected by the upper ocean circulation (Bjerknes 1964).

The goal of our study is to examine Bjerknes (1964) hypothesis that, on decadal time scales, fluctuations in the atmospheric northward heat transport and in the oceanic heat transport are out of phase, due to the slow adjustment of the oceanic currents to the winds. To this end, we formulate a minimal coupled model built on basic principles of conservation of heat and momentum.

Because in mid-latitudes the atmospheric northward heat flux is accomplished by eddies with zero zonal (and

time) mean, it is necessary, at least in the context of a simplified model, to parametrize their mean transport properties. To this end, we adopt the ideas of Green (1970) and Stone (1972) that the role of the eddies is to redistribute heat and potential vorticity in such a way as to reduce the large-scale gradients of these two scalar quantities.

In the ocean, the northward heat flux is mostly accomplished by the mean wind-driven circulation and by the mean meridional cell driven by the planetary thermohaline gradients. The former requires knowledge of the surface wind-stress, and thus of the flux of momentum exchanged between the atmosphere and the ocean. Given that there are no sources of angular momentum external to the Earth (neglecting the lunar interaction), the wind-stress is balanced by the lateral divergence of momentum flux, which is again dominated by the eddy transport. As shown by Green (1970), for quasi-geostrophic flows, it is possible to relate the zonally averaged eddy momentum flux to the mean potential temperature gradient, which in turn is determined by the global heat balance. Thus the interaction of the wind-driven circulation and the atmosphere requires the consideration of the heat and momentum budget of the coupled system.

The inclusion of the heat transport carried by the oceanic thermohaline circulation would require considering the moisture budget as well as the heat and momentum budgets. This is beyond the scope of the present study. To be sure, we also omit on purpose all the intrinsic variability of the separate atmospheric and oceanic systems.

The approach is along the same lines of Cessi (2000). However, here we make several simplifications which allow a firm understanding of the physics involved, while reproducing some of the features of the more complex model obtained in that reference. In particular, all the relevant oceanic and atmospheric fields oscillate with a decadal period.

## 2 The model

The model's geometry consists of one hemisphere with a single rectangular basin below a zonally averaged atmosphere of the same meridional extent. Thus, $0 < y < L_y$ is the latitudinal coordinate for both the atmosphere and the ocean. While the atmosphere occupies the whole hemisphere in the zonal direction, the ocean basin extends to a fraction, $r$, of the meridians, i.e., $0 < x < L_x$ is the zonal coordinate for the ocean and $0 < x < L_x/r$ is the zonal coordinate for the atmosphere.

We assume that the wind-driven oceanic flow is confined above the thermocline, i.e., for $-H < z < 0$, and we further assume that $H$ is a constant of the order of one kilometer.

In what follows the heat and mechanical balances of the atmospheric and oceanic parts are considered, and this leads to the set of equations that describe the model.

### 2.1 Oceanic mechanical balance: potential vorticity equation

Because our interest is in the wind-driven circulation, we consider the simplest model which describes the vertically averaged flow of waters above the permanent thermocline. Thus the evolution of the oceanic currents is described by the quasi-geostrophic equivalent barotropic potential vorticity equation on a mid-latitude $\beta$-plane. Because we are interested in motions on scales much larger than the oceanic baroclinic deformation radius, we neglect the relative vorticity contribution, so that the oceanic flow is governed by,

$$\frac{\partial \psi}{\partial t} - c\frac{\partial \psi}{\partial x} = \frac{R^2}{\rho_w H}\frac{\partial \tau_s}{\partial y} + c\delta\nabla^2\psi \quad . \tag{1}$$

Here, $\psi$ is the streamfunction averaged over the depth of the thermocline, $R$ is the baroclinic deformation radius and $c = \beta R^2$ is the speed of the long Rossby waves. $\rho_w$ is the sea-water density, $\tau_s$ is the zonal component of the atmospheric surface wind stress and $\delta \ll L_x$ is the width of the western boundary layer. The dissipative term is in the form of down-gradient potential vorticity diffusion, as appropriate for the parametrization of quasi-geostrophic eddies (Rhines and Young 1982).

Because we are considering a zonally averaged atmosphere, we identify $\tau_s$ with its zonal average, $\bar{\tau}_s(y,t)$. The streamfunction satisfies no flow conditions, $\psi = 0$, at the solid meridional boundaries, $x = 0, L_x$, and at the zonal boundaries at $y = 0, L_y$.

If $\delta \ll L_x$, the solution of (1) is the sum of the interior flow plus a western boundary layer correction:

$$\psi = \psi_I(x,y,t) - \psi_I(0,y,t)\exp(-x/\delta) + O(\delta) \quad . \tag{2}$$

$\psi_I$ is the interior streamfunction, which satisfies

$$\frac{\partial \psi_I}{\partial t} - c\frac{\partial \psi_I}{\partial x} = \frac{R^2}{\rho_w H}\frac{\partial \tau_s}{\partial y} \quad . \tag{3}$$

The solution of (3) is the sum of the forced response plus a solution, $\psi_h$, of the hyperbolic homogenous equation, with characteristics $x + ct$, that is

$$\psi_I = \frac{R^2}{\rho_w H}\int^t \frac{\partial \tau_s(y,t')}{\partial y}\mathrm{d}t' + \psi_h(x+ct) \quad . \tag{4}$$

Only the no normal flow condition at the eastern boundary can be enforced, and this determines $\psi_h$, so that the interior stream function is given by

$$\psi_I = \frac{R^2}{\rho_w H}\int_{t-(L_x-x)/c}^{t} \frac{\partial \tau_s}{\partial y}\mathrm{d}t' \quad . \tag{5}$$

In principle, additional boundary layers must be appended near the northern and southern boundaries in order to satisfy the no normal flow condition. However such boundary layers, unlike the western one, play no role in the dynamics of the main gyres, while they complicate the solution substantially. We thus neglect these boundary layer corrections, and confirm *a posteriori* that our results do not hinge on this approximation.

For later reference we denote with $\psi_w$ the streamfunction at the western edge of the interior, $\psi_w(y,t) \equiv \psi_I(0,y,t)$, which is given by:

$$\psi_w = \frac{R^2}{\rho_w H}\int_{t-L_x/c}^{t} \frac{\partial \tau_s}{\partial y}\mathrm{d}t' \quad . \tag{6}$$

Note that $\psi_w$ at the time $t$ is determined by the wind stress curl at the times from $t - L_x/c$ to the actual time $t$. $L_x/c$ is the time for a Rossby wave to cross the basin, independent of latitude in the quasigeostrophic approximation.

Equation (5) describes the baroclinic response of the ocean to an imposed wind-stress through the propagation of Rossby waves from the eastern boundary. As the wind stress varies in time, the ocean is continuously adjusting towards Sverdrup balance. Throughout the adjustment process, Rossby waves are generated at the eastern boundary, and they propagate westward the information about the wind that was blowing at the times when they were formed. Through (6), the ocean contains the memory of the state of the atmosphere back to the delayed time, $t - L_x/c$.

The following section details how to determine the zonally averaged wind-stress curl, $\partial\tau_s/\partial y$.

## 2.2 Atmospheric momentum balance: zonal momentum equation

A simple way to represent large-scale, mid-latitude, atmospheric dynamics is to examine the mean zonal flow. Specifically, we consider the zonally averaged $x$-momentum equation on a $\beta$-plane, which is given by

$$\frac{\partial\bar{u}}{\partial t} = f\bar{v} - \frac{\partial(\overline{uv})}{\partial y} + \frac{1}{\rho_a}\frac{\partial\bar{\tau}}{\partial z} \ . \tag{7}$$

The overbar indicates the zonal average, $f$ and $\rho_a$ are the local rate of rotation and atmospheric density respectively and $\bar{\tau}$ is the vertical flux of zonal momentum due to small-scale, turbulent eddies. Multiplying (7) by $\rho_a$ and integrating over the depth of the atmosphere, the first term on the right hand side vanishes because of mass conservation. Assuming that $\bar{u}$ is in equilibrium on decadal time scales, one finds:

$$-\int_0^\infty \rho_a \frac{\partial(\overline{uv})}{\partial y}\mathrm{d}z = \tau_s \ . \tag{8}$$

This equation represents the zonally and vertically averaged momentum budget for the atmosphere. The zonally averaged wind stress is balanced by the lateral convergence of momentum flux in the entire troposphere. The contribution to the momentum flux by the mean meridional circulation is observed to be much smaller than that due to the eddies in mid-latitudes, and it is very small even in the tropics. Therefore, to a very good approximation

$$\int_0^\infty \rho_a \overline{uv}\mathrm{d}z \approx \int_0^\infty \rho_a \overline{u'v'}\mathrm{d}z \ , \tag{9}$$

where the prime denotes departure from the zonal average. Thus the momentum balance requires knowledge of the statistical properties of the eddies. In the mid-latitudes, the eddy momentum flux accelerates the westerlies, so that a parametrization of the eddy momentum flux as diffusion down the mean zonal momentum gradient is not appropriate.

Green (1970) suggested using the relation between the zonally averaged quasigeostrophic eddy fluxes of momentum, heat and potential vorticity to relate the eddy momentum flux to zonally averaged quantities. The idea behind this strategy is that eddy heat and potential vorticity, unlike momentum, are conserved following particle motion, so that mixing length arguments can be applied. Denoting the potential vorticity with $q$, we have:

$$\rho_a(\overline{q'v'}) = -\frac{\partial\left[\rho_a(\overline{u'v'})\right]}{\partial y} + f_o\frac{\partial}{\partial z}\left[\frac{\rho_a}{S}(\overline{\theta'v'})\right] \ . \tag{10}$$

The potential vorticity is:

$$q = \beta y + v_x - u_y + \frac{f_o}{\rho_a}\frac{\partial}{\partial z}\left(\frac{\rho_a}{S}\theta\right) \ . \tag{11}$$

$\theta$ denotes the potential temperature and $S$ is the static stability of the atmosphere. The right hand side of (10) is the divergence of the Eliassen-Palm flux vector, and this relation allows the wind stress curl to be expressed in terms of $\bar{\theta}$ and $\bar{q}$.

### 2.2.1 Parametrization of eddy fluxes

Green (1970) proposes parametrization of the eddy fluxes in analogy with molecular diffusion. In this way the zonally averaged eddy flux of any conserved quantity is proportional to its zonally averaged gradient, and the flux divergence is:

$$\frac{\partial(\overline{q'v'})}{\partial y} = -\frac{\partial}{\partial y}\left(\kappa\frac{\partial\bar{q}}{\partial y}\right) \ , \tag{12}$$

$$\frac{\partial(\overline{\theta'v'})}{\partial y} = -\frac{\partial}{\partial y}\left(\kappa\frac{\partial\bar{\theta}}{\partial y}\right) \ . \tag{13}$$

$\kappa$ is the eddy diffusivity, i.e. the rate of change of mean square displacement of $\bar{\theta}$ and $\bar{q}$ due to geostrophic eddies. Different authors have proposed different forms of eddy diffusivity, $\kappa$, and a summary can be found in chapter 7 of Hoskins and Pearce (1983).

The validity of a local relation between the eddy fluxes and the mean gradients relies on a substantial separation between the average eddy size and the typical scale of the mean flow. In the atmosphere, mid-latitude baroclinic eddies are not very much smaller than the planetary scale, so it is not clear that the local down-gradient diffusion law is preferable to other mixing parametrizations which obey the same global conservation laws. We thus explore the possibility of parametrizing the divergence of the eddy fluxes as relaxation to the planetary average rather than downgradient diffusion, that is,

$$\frac{\partial(\overline{q'v'})}{\partial y} = \nu(\bar{q} - \bar{q}_A) \ , \tag{14}$$

$$\frac{\partial(\overline{\theta'v'})}{\partial y} = \nu(\bar{\theta} - \bar{\theta}_A) \ . \tag{15}$$

The subscript "$A$" stands for the meridional average and $\nu$ is the eddy relaxation rate. The simplified parametrization of eddy heat fluxes in (15), has been used in the early energy balance models (Budyko 1969). Lindzen and Farrell (1977) show that (13) and (15) lead to indistinguishable results. Encouraged by the comparison detailed in Lindzen and Farrell (1977), we adopt the same simplified parametrization in (14) for the potential vorticity eddy flux. The choice in (14) is in the same spirit as Green (1970) and Pavan and Held (1996), where the eddy fluxes of heat and potential vorticity are parametrized in the same fashion.

The zonally averaged potential vorticity can be expressed all in terms of the surface wind stress and the mean potential temperature, as long as the thermal wind balance holds, because

$$\bar{u} = \tau_s/C - g(f_o\Theta_0)^{-1}z\bar{\theta}_y \ . \tag{16}$$

In (16) $\Theta_0$ is the average temperature (in Kelvin) around which the Boussinesq approximation is pivoted, and $C$ is the drag coefficient relating the surface wind to the wind-stress. Here, we have assumed that the dynamical part of the potential temperature is independent of height as in a two-parameter formulation (Phillips 1963), which is analogous to a two-level model.

Following Green (1970), we posit that the eddy activity is maximum near the surface, and thus $\nu$ is taken of the form: $\nu = \nu_o\exp(-z/d)$, where $d$ is the eddy scale height.

Finally, the equation for the wind-stress curl is obtained by substituting (14) and (15) into (8). After using the identity (10) one finds:

$$\frac{\partial\tau_s}{\partial y}(1 + d_e\rho_o\nu_o/C) = d_e\rho_o\nu_o\left[\beta(y - \frac{L_y}{2}) + \frac{f_o}{Sd}(\bar{\theta} - \bar{\theta}_A + L_d{}^2\bar{\theta}_{yy})\right] \ . \tag{17}$$

Here we have taken a standard atmospheric density profile $\rho_a = \rho_o\exp(-z/D)$, and we have defined the effective eddy scale-height: $d_e{}^{-1} = D^{-1} + d^{-1}$. With this notation, the effective baroclinic deformation radius, $L_d$, is defined as

$$L_d = [dd_egS/(f_o^2\Theta)]^{1/2} \ . \tag{18}$$

For the sake of simplicity, we could not resist the temptation of neglecting the relative vorticity contribution to the wind-stress [the terms proportional to $L_d^2$ in (17)]. This approximation is accurate on the scale of a hemisphere because $(L_d/L_y)^2$ is much smaller than unity ($d_e \approx D/3$, in the calculations discussed in Sect. 3). Consistently, we also neglect the contribution due to the surface wind [this is the term inversely proportional to $C$ in (17)]. Thus our approximate equation for the wind-stress curl is

$$\frac{\partial \tau_s}{\partial y} \approx d_e \rho_o v_o \left[ \beta \left( y - \frac{L_y}{2} \right) + \frac{f_o}{Sd} (\bar{\theta} - \bar{\theta}_A) \right] \ . \tag{19}$$

The wind stress can be obtained from (19) by integrating in $y$ and enforcing the boundary conditions $\tau_s = 0$ at $y = 0, L_y$. Notice that it is possible to apply these two boundary conditions because the integral over the domain of the right hand side of (19) vanishes. We further require that there is no net stress over the hemisphere, i.e., $\int_0^{L_y} \tau_s \mathrm{d}y = 0$. This additional constraint determines the eddy scale height $d$ in terms of the integral distribution of $\bar{\theta}$. The wind stress curl is thus entirely determined by the zonally average surface potential temperature $\bar{\theta}$. An expression for this variable is found by considering the atmospheric heat budget, which is the next step in the model's formulation.

### 2.3 Atmospheric heat balance: potential temperature equation

In the spirit of Stone (1972) and Vallis (1980, 1982), $\bar{\theta}$ is determined by the zonally averaged thermodynamic energy equation for the atmosphere:

$$\frac{\partial \bar{\theta}}{\partial t} = -\frac{1}{\rho_a} \frac{\partial (\rho_a \overline{\theta w})}{\partial z} - \frac{\partial (\overline{\theta v})}{\partial y} + \frac{1}{C_{pa} \rho_a} \frac{\partial \bar{Q}}{\partial z} \tag{20}$$

where $C_{pa}$ is the specific heat and $\bar{Q}$ is the diabatic heat flux. The typical response time of atmospheric potential temperature to variations in heat fluxes is of the order of weeks, which is much shorter than the typical time scales of evolution of upper ocean temperature (of the order of years). It is therefore permissible to neglect the time derivative of $\bar{\theta}$ and assume that the atmosphere adjusts instantaneously to the ocean. Integrating (20) vertically, a balance is obtained between the horizontal heat flux divergence in the troposphere and the net diabatic heat fluxes at the vertical boundaries, that is,

$$C_{pa} \int_0^\infty \rho_a \frac{\partial (\overline{\theta v})}{\partial y} \mathrm{d}z = F - r\lambda (\bar{\theta} - \bar{T}_s) \ . \tag{21}$$

Here $F$ represents the net radiative incoming flux at the top-of-the-atmosphere and it is given by the difference between the net incoming solar radiation, $F_{SOLAR}$ and the outgoing long-wave radiation, $F_{LONG\text{-}WAVE}$. The incoming radiation is a prescribed function of latitude chosen to be,

$$F_{SOLAR} = F_o + \tilde{F}_1(y) \ , \tag{22}$$

where $\tilde{F}_1$ has zero latitudinal average. The outgoing longwave radiation is estimated by linearizing the gray Stefan-Boltzmann law and is given by,

$$F_{LONG\text{-}WAVE} = A + B\bar{\theta} \ . \tag{23}$$

The second term on the right hand side of (21) denotes the exchange of heat flux at the air-sea interface. We use a typical bulk formula which empirically approximates the complex heat exchange processes at the sea surface with relaxation to the zonally averaged sea surface temperature, $\bar{T}_s$. $\lambda$ is the bulk transfer coefficient, assumed constant, and $r$ is the fraction of a latitude circle covered by oceans.

The vertically and zonally averaged poleward heat transport is dominated in the mid-latitudes by eddies with no zonal mean, while in the tropics the mean meridional circulation also contributes. Nevertheless, because our focus is on mid-latitude dynamics we assume that $\overline{\theta v} \approx \overline{\theta' v'}$ and use the non-local parametrization (15). In any case, (15) acts to reduce the pole to equator temperature gradient which is the same effect achieved by both the mean meridional circulation and the mid-latitude transient eddies. The final expression for the zonally averaged atmospheric potential temperature is

$$(\bar{\theta} - \bar{\theta}_A) = (1 - a) \left[ (\bar{T}_s - \bar{\theta}_A) + \frac{\tilde{F}_1}{r\lambda} \right] \tag{24}$$

where $0 < a < 1$, is given by $a^{-1} = 1 + r\lambda / (C_{pa} v_o \rho_o d_e + B)$. The planetary averaged surface potential temperature is determined solely by radiative processes and is given by

$$\bar{\theta}_A = (F_o - A)/B \ . \tag{25}$$

The final step needed to close the system is to find an expression for the sea surface temperature, $T_s$.

### 2.4 Oceanic heat balance: upper ocean heat content equation

The oceanic temperature is determined by considering the heat balance of the upper ocean, and neglecting the exchange of heat between the thermocline and the deeper water. Moreover, we assume that the temperature $T$ of the oceanic layer is independent of depth ($T = T_s$). The vertically integrated heat balance equation is:

$$\frac{\partial T}{\partial t} + \frac{\partial (uT)}{\partial x} + \frac{\partial (vT)}{\partial y} = \frac{\lambda}{C_{pw} \rho_w H} (\bar{\theta} - T) + \epsilon \nabla^2{}_h T \ . \tag{26}$$

Where $(u, v) = (-\psi_y, \psi_x)$ is the wind-driven velocity and $\epsilon$ is the eddy diffusivity due to mesoscale oceanic motion. Note that, except for the western boundary layer balance, this is the only explicitly diffusive term in the model. Without diffusion, the warm waters transported poleward by the subtropical gyre and the cold waters transported equatorward by the subpolar gyre would form a discontinuous front at the gyre boundary. In the present formulation, diffusion is the only means of direct communication between the gyres which are otherwise connected through the atmosphere. Because the scale of oceanic baroclinic eddies is much smaller that the planetary scale, a local relation between the eddy-heat flux and the mean temperature gradient is on firmer ground than in the atmospheric analogue.

Since the atmospheric model is only influenced by the zonally averaged oceanic temperature, the natural way to proceed is to separate $T$ into the zonal average, $\bar{T}$, and the departure from the zonal average, $T'$. The upper ocean heat content (26) can then be divided into the two coupled equations:

$$\frac{\partial \bar{T}}{\partial t} + \frac{\partial (\overline{vT'})}{\partial y} = \frac{\lambda a}{C_{pw} \rho_w H} \left[ \bar{\theta}_A - \bar{T} + \frac{\tilde{F}_1 (1 - a)}{r\lambda a} \right] + \epsilon \frac{\partial^2 \bar{T}}{\partial y^2} \ , \tag{27}$$

$$\frac{\partial T'}{\partial t} + u \frac{\partial T'}{\partial x} + v \frac{\partial T'}{\partial y} - \frac{\partial (\overline{vT'})}{\partial y} + \frac{\lambda}{C_{pw} \rho_w H} T' - \epsilon \nabla^2{}_h T' = -v \frac{\partial \bar{T}}{\partial y} \ . \tag{28}$$

In (27), (24) has been used to write $\bar{\theta}$ as a function of $\bar{T}$.

#### 2.4.1 Simplification in the rapid relaxation limit

Comparison of (27) and (28) reveals two fundamental differences between $\bar{T}$ and $T'$. Firstly, the relaxation rate for $\bar{T}$ is smaller than that for $T'$ by the factor $a$ (<1). This is because the zonally averaged atmospheric potential temperature depends directly on $\bar{T}$, but not on $T'$. Therefore, on the time scales over which $\bar{T}$ changes, $T'$ rapidly reaches equilibrium. Secondly, while $\bar{T}$ is directly forced by radiation through its interaction with the atmosphere, longitudinal differences in ocean temperature, $T'$, are only forced by advection of zonally averaged temperature gradients [the last term on the left hand side of (28)]. It is thus clear that $T'$ must be proportional to $v\bar{T}_y$. In the limit $v/L_y \ll \lambda / (C_{pw} \rho_w H)$, we obtain the balance

$$v \frac{\partial \bar{T}}{\partial y} \approx -\frac{\lambda}{C_{pw} \rho_w H} T' \ . \tag{29}$$

The diagnostic relation (29) allows us to express the zonally averaged heat flux divergence in terms of the zonally averaged temperature gradient, $\bar{T}_y$ (Wang et al. 1995), through the relation

$$\frac{\partial (\overline{vT'})}{\partial y} \approx -\frac{C_{pw} \rho_w H}{\lambda} \frac{\partial}{\partial y} \left( \overline{v^2} \frac{\partial \bar{T}}{\partial y} \right) \ . \tag{30}$$

The effect of meridional advection by the gyres on the zonally averaged temperature is to diffuse temperature down the mean

gradient with a diffusivity proportional to $\overline{v^2}$. The approximation leading to (30) predicts a quadratic dependence of the heat flux on the velocity. In fact, Wang et al. (1995) show that in the range where $v/L_y \gg \lambda/(C_{pw}\rho_w H)$ (30) loses its validity and the northward flux decreases with increasing velocity. For the parameter values that we use later, the maximum western boundary layer velocity satisfies $v/L_y \approx \lambda/(C_{pw}\rho_w H)$, so that we are at the edge of the range of validity of (30). Nevertheless, this approximation captures the qualitative dynamics, while allowing a remarkable simplification.

An additional simplification is obtained by noticing that $\overline{v^2}$ is dominated by the western boundary layer contribution, so that to first order in $\delta/L_x$ we have

$$\overline{v^2} \simeq \frac{{\psi_w}^2}{2\delta L_x} \ . \tag{31}$$

The final evolution of the oceanic temperature is,

$$\frac{\partial \bar{T}}{\partial t} - \frac{C_{pw}\rho_w H}{2\lambda\delta L_x}\frac{\partial}{\partial y}({\psi_w}^2\frac{\partial \bar{T}}{\partial y})$$

$$= \frac{\lambda a}{C_{pw}\rho_w H}\left[\bar{\theta}_A - \bar{T} + \frac{\bar{F}_1(1-a)}{r\lambda a}\right] + \epsilon\frac{\partial^2 \bar{T}}{\partial y^2} \tag{32}$$

with boundary conditions of no normal heat flux, $\bar{T}_y = 0$ at $y = 0, L_y$.

The interior streamfunction at the western boundary, $\psi_w$ is given in (6), and is entirely determined by $\bar{\tau}_y$. The wind-stress curl is given by (19), and thus directly proportional to $\bar{T}$ through (24).

### 2.5 Final set of equations

In order to determine what parameters effectively control the dynamics of the system thus derived, we nondimensionalize with the following choices:

$$y = L_y y^* \ , \tag{33}$$

$$t = \frac{C_{pw}\rho_w H}{\lambda} t^* \ , \tag{34}$$

$$(\bar{\theta} - \bar{\theta}_A, \bar{T} - \bar{\theta}_A) = \frac{F_1}{r\lambda}(\theta^*, T^*) \ , \tag{35}$$

$$\psi_w = \frac{D\rho_o v_o L_y L_x}{\rho_w H}\psi^* \ , \tag{36}$$

$$\tau_s = D\rho_o v_o \beta {L_y}^2 \tau^* \ . \tag{37}$$

In (35), $F_1$, is the amplitude of the radiative forcing, given by $F_1 = F_1 F(y)$, where $F(y)$ is a dimensionless function with a maximum value of unity.

We also substitute the diagnostic relations (24) and (19) into (6), and thus we obtain two coupled evolution equations relating the zonally averaged oceanic temperature and the oceanic streamfunction at the seaward edge of the western boundary. Dropping the asterisks from now on, we have:

$$\frac{\partial T}{\partial t} = \mu\frac{\partial}{\partial y}\left(\psi^2\frac{\partial T}{\partial y}\right) - aT + (1-a)F(y) + \sigma\frac{\partial^2 T}{\partial y^2} \ , \tag{38}$$

$$\psi = \frac{1}{t_o}\int_{t-t_o}^{t} \hat{d}(y - \frac{1}{2}) + \gamma(1-a)(1-\hat{d})$$

$$\times [F(y) + T(y,t')]\mathrm{d}t' \ . \tag{39}$$

In (38) and (39) the following definitions have been made:

$$F(y) = \cos(\pi y) \tag{40}$$

$$\gamma = \frac{f_o}{SD}\frac{F_1}{r\lambda\beta L_y} \tag{41}$$

$$\mu = \left(\frac{DC_{pw}\rho_o v_o}{\lambda}\right)^2 \frac{L_x}{2\delta} \tag{42}$$

$$\sigma = \frac{\epsilon C_{pw}\rho_w H}{\lambda(L_y)^2} \ , \tag{43}$$

$$\hat{d} = \frac{d_e}{D} \ , \tag{44}$$

$$a = \frac{B + C_{pa}v_o\rho_o D\hat{d}}{r\lambda + B + C_{pa}v_o\rho_o D\hat{d}} \ , \tag{45}$$

$$t_o = \frac{\lambda L_x}{C_{pw}\rho_w H c} \ . \tag{46}$$

$t_o$ is the non-dimensional delay time given by the ratio of the Rossby wave crossing time and the oceanic temperature decay time. The nondimensional eddy scale height, $\hat{d}$, is determined by enforcing the condition of no net surface torque instantaneously and is thus a function of time, as is $a$ through its dependence on $\hat{d}$. However, it turns out that $\hat{d}$ has a much weaker time-dependence than $T$ and $\psi$. $a^{-1}$ measures the time that the zonally averaged oceanic temperature would take to reach equilibrium with the atmospheric temperature in the absence of oceanic motion.

The parameter that controls the coupling between the wind-driven flow, $\psi$, and the ocean temperature, $T$, is $\mu$. In the limit $\mu \to 0$, the system reaches an equilibrium where $\theta = T$, and there is no oceanic heat transports (except for the small contribution due to the temperature diffusion), and thus no heat exchange between the two fluids. In Sect. 4 we examine the qualitative behavior of the solutions of (38) and (39) as a function of the coupling parameter, $\mu$.

The rapid relaxation limit leading to (30) offers several advantages over the formulation used by Cessi (2000). First, the final set of equations is much simpler, because there are only two variables, $\psi$ and $T$, that depend on the single spatial dimension, $y$. The dimensional reduction implies that the thin western boundary layer needs not to be resolved. Second, the space of parameters is substantially reduced: the final set (38) and (39) depend on the five nondimensional parameters, $a, \gamma, \mu, \sigma, t_o$, while the original formulation depends on many more.

Third, and most importantly, the system (38) and (39) shows that there is a feedback of the upper ocean heat content, $T$, onto the wind driven flow, $\psi$, mediated by the atmosphere through the requirements of global heat and momentum balance. Specifically, the role of the wind-driven gyres is to transport heat down the zonally averaged ocean temperature gradient, with a diffusivity, proportional to $\psi_w^2$, determined by the time history of $T$, all the way back to the delayed time $t - t_o$.

## 3 An oscillatory solution

The system (38) and (39) is solved numerically using the Crank-Nicholson scheme for the time stepping of the temperature equation, with centered differences for the spatial derivatives. The integral in time in (39) is discretized with the trapezoidal rule. At each time step, $t_n$, the knowledge of the temperature field at times from $t_n - t_o$ to $t_n$ is required. The radiative equilibrium temperature is used as the initial guess and it is assumed that the previous history of the temperature field, when unknown, is constant in time and equal to the initial condition.

The parameters pertaining to the atmosphere have values tuned to the mid-latitude Northern Hemisphere,

and those pertaining to the ocean are chosen to resemble the mid-latitude North Pacific. In this ocean, most of the heat is transported by the flow above the main thermocline, suggesting that the wind-driven gyres, rather than the thermohaline circulation, are responsible for the bulk of the oceanic heat budget. The parameter values used in this calculation are listed in Table 1.

The solution settles into a final state, independent of the initial condition, characterized by a periodic oscillation of all fields, with a period of 40 years.

### 3.1 The time averaged fields

Figure 1 shows different fields averaged over one period of the oscillation, as a function of latitude. The radiative forcing is perfectly symmetric about the middle of the domain and this symmetry is reflected in the solutions. The first and second top panels of Fig. 1 show the zonally averaged surface temperature of the ocean and atmosphere respectively. For reference, the equator to pole temperature difference in radiative equilibrium is 100 °C. The oceanic flow convergence at the subpolar and subtropical gyres boundary (located at $y = 5000$ km) induces a local sharpening of the temperature gradient.

The third top panel shows $\psi_w$, with the subtropical and subpolar gyres antisymmetric about the central latitude of the domain. For reference, a snapshot of the streamfunction, $\psi(x, y, t)$, is shown in Fig. 2. The maximum transport in the subtropical gyre, here 6 Sv, is substantially smaller than that observed for the North Pacific, which peaks at about 40 Sv. Thus the velocity in the western boundary layer reaches the maximum value $\psi_w/\delta = 0.12\,\mathrm{m/s}$. We are now in a position to test the validity of the rapid relaxation approximation (29): the ratio $\psi_w C_{pw}\rho_w H/(L_y\delta\lambda)$ is everywhere less than 1.6. Therefore, although perhaps not accurate, the rapid relaxation approximation does not grossly violate the premises upon which it is based.

The zonally averaged atmosperic (AHF) and oceanic (OHF) northward heat transports are plotted in the first and second bottom panels of Fig. 1, respectively. From (15), (30) and (31), AHF and OHF are given by

$$\mathrm{AHF} = C_{pa}\rho_o d_e v_o \int_0^y (\bar{\theta} - \bar{\theta}_A)\, \mathrm{d}y' \ , \tag{47}$$

$$\mathrm{OHF} = -C_{pw}\rho_w H\left(\frac{C_{pw}\rho_w H}{2\lambda\delta L_x}\psi_w^2 + \epsilon\right)\frac{\partial \bar{T}}{\partial y} \ . \tag{48}$$

**Table 1** Parameter values for the solution discussed in Sect. 3

| | | | |
|---|---|---|---|
| $L_x = 8.25 \times 10^6$ m | $\rho_o = 1.25$ kg m$^{-3}$ | $F_o - A = 371.25$ W m$^{-2}$ | $S = 5 \times 10^{-3}$ K m$^{-1}$ |
| $L_y = 10^7$ m | $\rho_w = 1000$ kg m$^{-3}$ | $B = 2.5$ W m$^{-2}$ K$^{-1}$ | $\beta = 2 \times 10^{-11}$ m$^{-1}$ s$^{-1}$ |
| $H = 10^3$ m | $C_{pa} = 1000$ J K$^{-1}$ kg$^{-1}$ | $F_1 = 125$ W m$^{-2}$ | $f_o = 10^{-4}$ s$^{-1}$ |
| $\delta = 5.1 \times 10^4$ m | $C_{pw} = 4000$ J K$^{-1}$ kg$^{-1}$ | $\lambda = 30$ W m$^{-2}$ K$^{-1}$ | $R = 2.8 \times 10^4$ m |
| $D = 10^4$ m | $v_o = 5 \times 10^{-7}$ s$^{-1}$ | r = 0.3 | $\epsilon = 1 \times 10^3$ m$^2$ s$^{-1}$ |

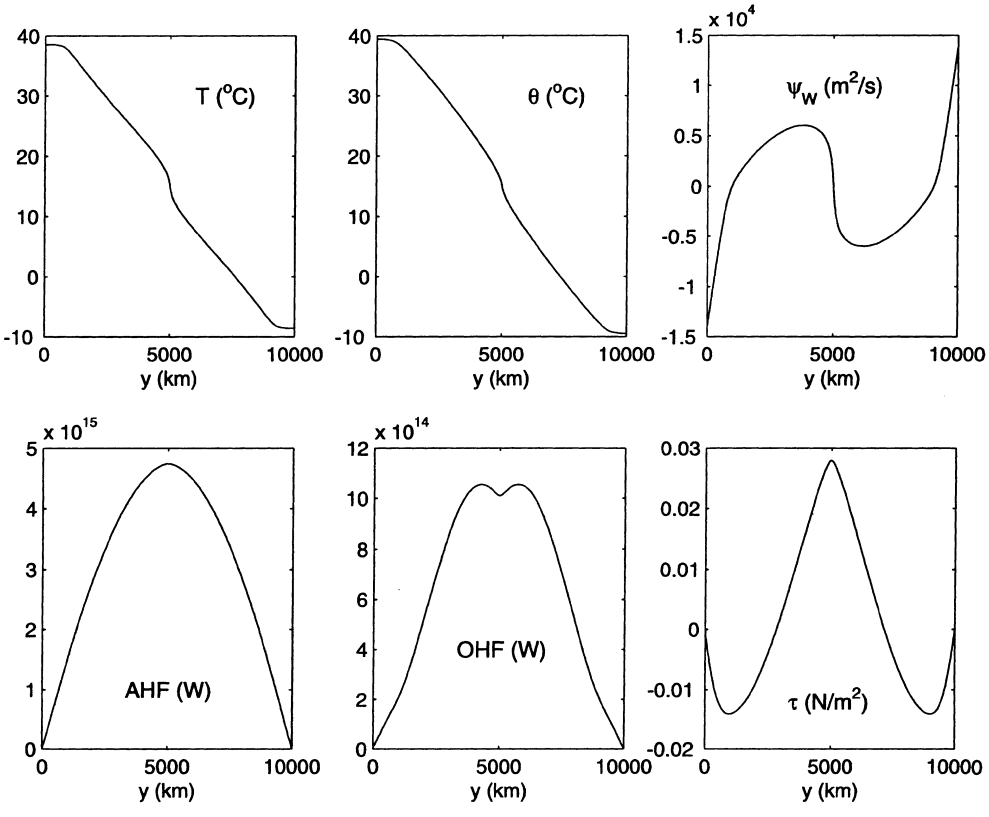


**Fig. 1** The zonally averaged temperature, $\bar{T}$, potential temperature, $\bar{\theta}$, and the western boundary interior streamfunction, $\psi_w$ (*top row*). The atmospheric, *AHF*, and oceanic, *OHF*, northward heat transports and the wind-stress, $\tau_s$, (*bottom row*). All fields are averaged over one period of the oscillation. The parameter values for Figs. 1–5 are given in Table 1, and the effective eddy scale height is $d_e = 3.68 \times 10^4$ m

Here we have included the contribution to the oceanic heat transport due to the explicit diffusion. This term is responsible for all the heat transport at the intergyre boundaries, and it is subdominant elsewhere.

Although the wind-stress (third bottom panel in Fig. 1) and Sverdrup flow are substantially weaker than those observed in the North Pacific, the zonally averaged atmospheric and oceanic northward transports peak at values that are consistent with the current estimates from data (Trenberth and Solomon 1996). Because our model is constructed to conserve global heat and momentum, we are reassured that, despite the severe simpifications, the basic physical process of heat and momentum exchange are correctly captured.

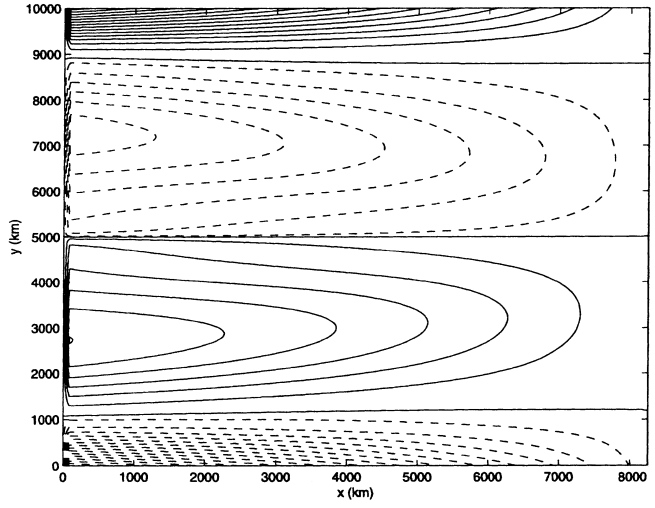


**Fig. 2** A snapshot of the streamfunction, $H\psi$, as a function of $x$ and $y$. The contour interval is one Sverdrup (1 Sv = $10^6\,\mathrm{m}^3/\mathrm{s}$) and negative contours are *dashed*. The maximum transport in the subtropical gyre is 6 Sverdrups. The field can be obtained diagnostically using the approximations (2) and (5)

## 3.2 The anomalies

Figure 3 shows the departures of $\bar{T}$ (left panel) and $\psi_w$ (right panel) from the time mean as a function of latitude and time. The period of the oscillation is approximately 40 years, and we plot two periods. As detailed in the next section the period is linearly proportional to the long Rossby wave transit time, which is $L_x/c = 16.7$ years for the parameter values given in Table 1. The temperature and transport anomalies are antisymmetric about the central latitude of the domain and occupy the entire latitudinal extent of the subtropical and subpolar gyres. Consistent with our approximation that the western boundary velocity dominates the temperature advection, the anomalies propagate towards the gyre boundary.

Notice that the fluctuations in $\bar{T}$ are in approximate quadrature with the oceanic transport anomalies. This property is clearly illustrated in Fig. 4, where the $\bar{T}$ and $\psi_w$ anomalies are plotted as a function of time, for the latitude $y = 4000$ km, located in the subtropical gyre. The anomalies have been normalized by their maximum value.

Consider the point in time in which there are no temperature anomalies (solid line) and the circulation in

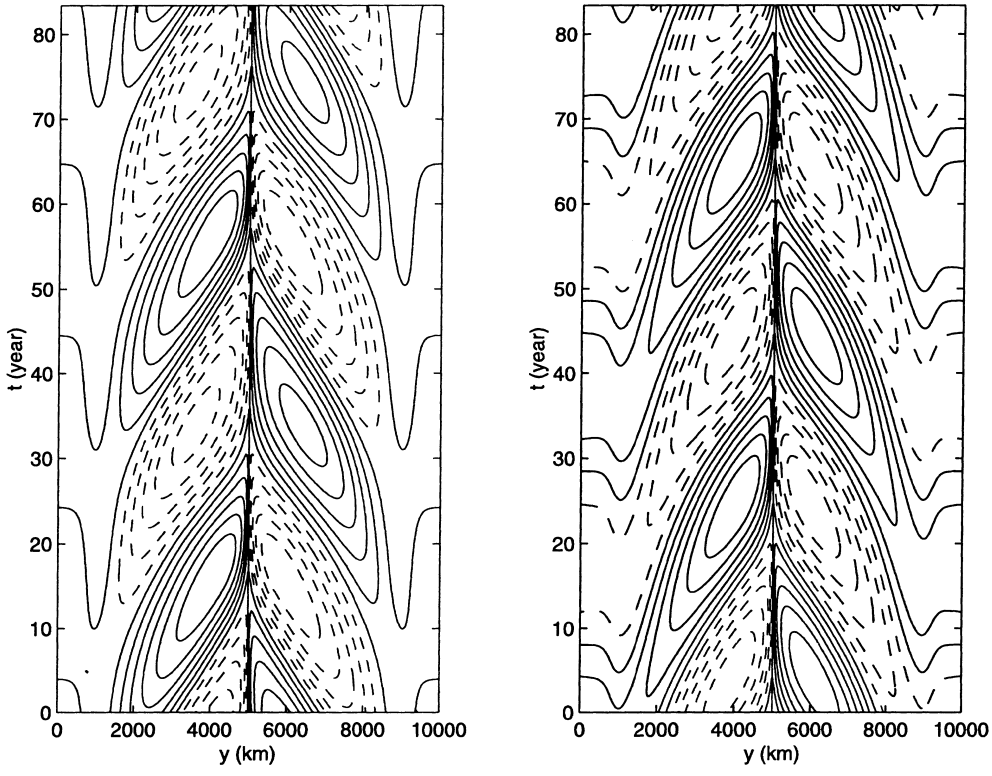


**Fig. 3** The departures from the time mean fields of $\bar{T}$ (*left panel*) and $\psi_w$ (*right panel*), as a function of latitude and time during two periods of the oscillation. Negative values are *dashed* and the contour interval is 0.33 °C for temperature, and 491 $\mathrm{m}^2/\mathrm{s}$ for $\psi_w$. The maximum value of the temperature anomalies is 2 °C, while the maximum value of the western boundary streamfunction is $3 \times 10^3\,\mathrm{m}^2/\mathrm{s}$

the gyres (dashed line) is weak. This corresponds to point A in Fig. 4. As time goes on, the subtropical gyre becomes warmer while the subpolar gyre becomes colder (point B in Fig. 4). This implies an increase in the wind-stress curl in both gyres. If the ocean responded instantaneously to the changed wind-stress, the resulting stronger circulation in the gyres would increase the oceanic heat transport opposing the temperature anomaly and a steady equilibrium would be reached. However, because of the long Rossby wave delay, the velocity in the gyres depends not only on the actual, increased wind-stress but also on the wind-stress which was forcing the ocean in the past 17 years. At that time, there was a negative temperature anomaly in the subtropical gyre and a positive one in the subpolar gyre and therefore a reduced wind-stress curl. The reduced velocity allows the temperature anomaly to grow until about 10 years later, when the effect of the increased temperature spins up the gyre. Thus, it is not until some years later, that the oceanic circulation anomaly starts changing sign in response to the variations in temperature (point C in Fig. 4). As the circulation becomes stronger, it begins to reduce the temperature anomaly and eventually changes its sign. Then, the second phase of the oscillation starts, (point D in Fig. 4).

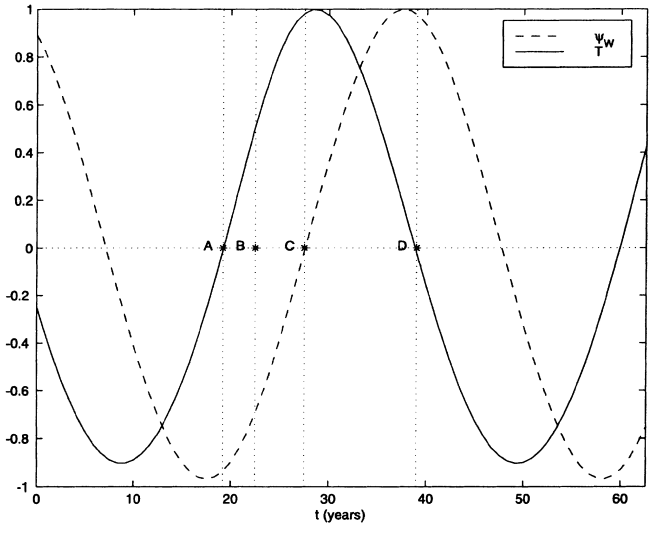


**Fig. 4** The anomaly of $\bar{T}$ (*solid line*) and $\psi_w$ (*dashed line*) at the latitude $y = 4000$ km as a function of time. Both quantities have been normalized to their maximum value. The two fields are in approximate quadrature

The storage term in the oceanic temperature equation [$\partial T/\partial t$ in (38)] plays an important role. Without it, the oceanic temperature and boundary current transport anomalies would be in exact quadrature.

In Fig. 5 the fluctuations of zonally averaged oceanic (left panel) and atmospheric (right panel) northward heat transport are shown. As originally suggested by Bjerknes (1964), the two components of the heat transport oscillate approximately out of phase. Because the changes in radiation are negligible compared to those in the transport, if the rate of change of oceanic heat storage were negligible, the amplitude of these two components should be equal. However, the AHF anomalies are over a factor of four smaller than the

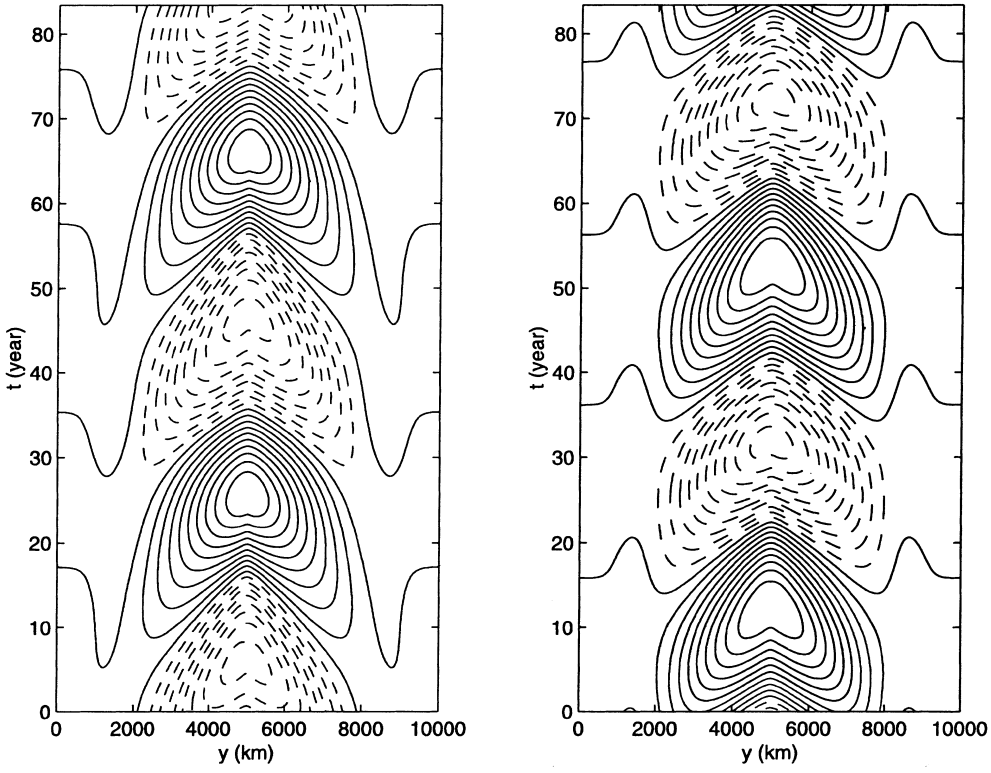


**Fig. 5** The departures from the time mean of the zonally averaged oceanic (*left panel*) and atmospheric (*right panel*) northward heat transport, as a function of latitude and time. Negative values are *dashed* and the contour interval is $8.7 \times 10^{13}$ W for OHF and $1.97 \times 10^{13}$ W for AHF. The maximum value of the OHF anomalies is $6.1 \times 10^{14}$ W and the maximum value of the AHF anomaly is $1.38 \times 10^{14}$ W. The two anomalies are not in antiphase, because the ocean heat storage rate (not shown) is as large as the heat transport anomalies

OHF anomalies. Indeed, the rate of oceanic heat storage (not shown here), accounts for the difference between the fluctuations in AHF and OHF. Thus, our model indicates that on decadal time scales the oceanic heat storage plays a role as important as the northward transports in the global heat budget.

## 4 Parameter exploration

In this section we explore how the solutions of (38) and (39) depend on two of the control parameters, the delay $t_o$ and a measure of the oceanic circulation's strength, $\mu$, defined in (42).

The top panel of Fig. 6 shows that the period of the oscillation is linearly proportional to the long Rossby wave delay, $L_x/c$. Variations in the delay time, keeping all the other parameters fixed are obtained by varying the Rossby deformation radius of the ocean, $R$. As is common in simple delay systems with "negative feedbacks" (Glass and Mackey 1988), when the delay is shorter than the negative feedback rate the oscillations are damped and the system approaches a steady state as $t \to \infty$. This is illustrated in the middle panel of Fig. 6 where the decay rate of the oscillation is plotted as a function of the delay, $L_x/c$. The decay rate is computed assuming that the amplitude of the oscillation decays exponentially, and is evaluated at the coordinate $y$ where the oceanic temperature anomaly is maximum. For delays above a critical value, about 10 years for these parameter values, the decay rate is zero and the oscillations are sustained thus reaching a finite amplitude.

The dependence of the amplitude on the delay is shown in the bottom panel of Fig. 6. As a measure of the amplitude of the oscillation we computed the following index

$$\text{amplitude} \equiv \frac{\max_y(\bar{T} - \langle\bar{T}\rangle) - \min_y(\bar{T} - \langle\bar{T}\rangle)}{\max_y(\langle\bar{T}\rangle) - \min_y(\langle\bar{T}\rangle)} \quad , \qquad (49)$$

where the angle brackets indicate the time average. For delays less than the critical value, there are no sustained oscillations and the system reaches a steady state. As the critical threshold is passed, the system settles on a limit cycle, with solutions whose spatial characteristics are exemplified in the previous section. Interestingly, as the delay becomes longer the oscillations are always sustained, but their nonlinearly equilibrated amplitude becomes vanishingly small as $t_o$ is increased. This is typical of "negative feedback" systems with delay, for which the growth rate of infinitesimal perturbations around the unstable steady state is inversely proportional to the delay, in the limit of long delays (Manneville 1990). Intuitively, this is because when the delay becomes very long, the relaxation of the oceanic temperature towards the atmospheric temperature [the second term on the right hand side of (38), fixed at 8.5 years for this calculation] damps the transport perturbations before they can reach the western boundary and change the atmospheric temperature and the wind-stress curl.

In Fig. 7 the stability of the periodic solution is examined as a function of the parameter, $\mu$, which controls

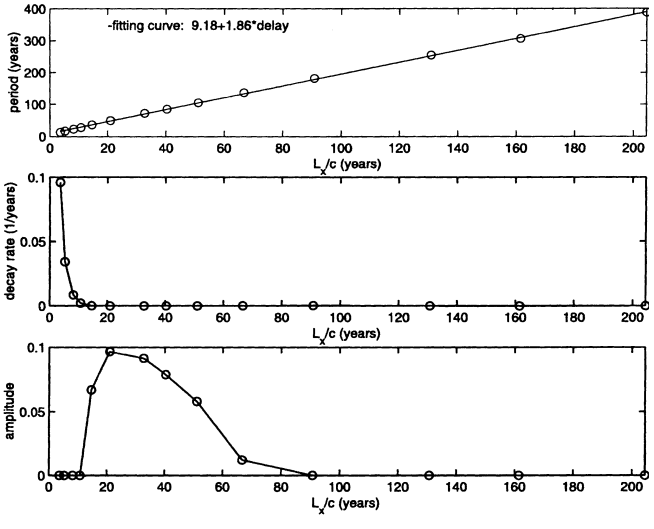


**Fig. 6** Qualitative behaviour of the solution as a function of the delay time, $L_x/c$, which is varied by changing the value of the oceanic Rossby deformation radius, $R$. All the other parameters have the values given in Table 1. The *top panel* shows the oscillation period obtained by solving (38) and (39) (*open circles*), and the linear best fit (*solid line*), which holds for two decades of delay values. In the *middle panel* a measure of the exponential decay rate of the periodic solutions is plotted. For delays longer than about 10 years the solution reaches a limit cycle and the decay rate is zero. Below the critical delay the oscillations are damped and eventually a steady state is reached. The *bottom panel* shows the amplitude of the oscillation, defined in (49). For delays less than the critical value the system reaches a steady state and the amplitude is zero. For very long delays, although the oscillations are sustained, their amplitude becomes infinitesimal

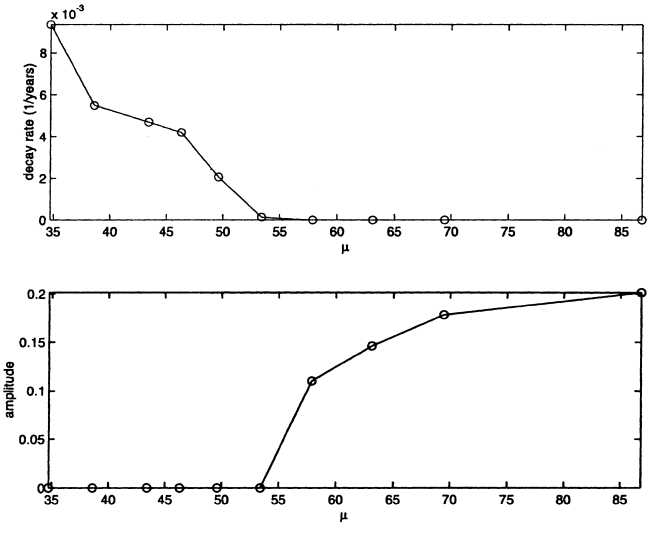


**Fig. 7** Qualitative behaviour of the solution as a function of the strength of the oceanic circulation, $\mu$, defined in (42). $\mu$ is varied by changing the width of the western boundary layer, $\delta$, while keeping all the other parameters fixed to the values listed in Table 1. The *top panel* shows the exponential decay rate, while the *bottom panel* shows the amplitude, defined in (49). For "delayed negative feedback" below a critical value the system reaches a steady state

the importance of the oceanic northward heat transport in the global heat balance. This parameter is varied, while keeping all others fixed, by decreasing the width of the western boundary current, $\delta$, from 82.5 km to 33 km. It is clear that $\mu$ must exceed a critical threshold for the oscillations to be sustained. The solution detailed in Sect. 3 is at the point $\mu = 55.5$, so it just passed the threshold of a sustained oscillation. Remarkably, the period (not shown) varies by only a few percent for the range of $\mu$ explored, indicating that the nonlinear correction to the frequency is weak.

The linear dependence of the oscillations' period on the delay, $L_x/c$, is a qualitative departure from the results obtained by Cessi (2000). In that case the period of the oscillations is proportional to the geometric average of $L_x/c$ and the advective time, $L_x^2/\psi_w$. Presumably, because here we take the rapid relaxation, weak advection limit the latter time scale does not enter in the dynamics.

## 5 Summary and conclusions

An idealized model of the coupled large-scale dynamics of the mid-latitude atmosphere and the wind-driven ocean circulation has been formulated. Simplified eddy parametrizations, which conserve global momentum and heat, have been used to relate the heat and momentum eddy fluxes in the atmosphere to the zonally averaged oceanic and atmospheric temperatures. In our formulation, the ocean and the zonally averaged atmosphere are coupled through wind stress and heat fluxes at the air-sea interface.

We exploit the smallness of the advection time compared to the relaxation time of the longitudinally varying part of the ocean temperature, and the thinness of the western boundary layer compared to the basin width. In this limit, the two-dimensional ocean formulation can be reduced to one-dimensional evolution equations for the zonally averaged ocean temperature and for the interior ocean velocity. The approximation nicely illustrates that the role of the northward heat flux by the ocean gyres is to redistribute heat down the mean oceanic temperature gradient.

Although the feedback between the ocean gyres and the wind-stress is negative, the delayed response of the oceanic velocity to the wind-stress curl leads to sustained oscillations at decadal time scales. The period of the oscillation is dictated by the transit time of long Rossby wave across the basin. The spatial structure is characterized by large-scale anomalies, as originally assumed when deriving the simplified set of dynamics. This is an aspect of the present results which agrees with the numerical computations of Latif and Barnett (1994, 1996). However, Latif and Barnett (1994, 1996) invoke a local feedback mechanism between the wind and the sea surface temperature (through the dependence of the mixing coefficient on wind speed), which is absent in our model.

Unlike the mechanism proposed by Jin (1997) and Weng and Neelin (1998), the oscillations resulting from the coupled model presented here do not rely on the excitation of an oceanic basin mode by a wind-stress of the appropriate longitudinal scale. In our case the wind-stress has no structure in the zonal direction. This choice is forced upon us by the desire to use physically based parametrizations of atmospheric eddy heat and momentum fluxes and their role in reshaping the large-scale atmospheric circulation.

Within the context of a simple but consistent model, where heat and momentum are globally conserved, we verify the Bjerknes' (1964) conjecture that the oceanic and atmospheric components of the northward heat transport fluctuate out of phase. The Bjerknes' mechanism is robust to the inclusion of oceanic heat storage rate, which alters quantitatively, but not qualitatively, the division of heat transport fluctuations between the atmosphere and the ocean. Thus, we conclude that coupled modes of variability should exist on our planet unless:

1. The processes controlling radiative equilibrium, such as cloud coverage, have low frequency variability of magnitude larger than the transport terms in the global heat budget.
2. The intrinsic low frequency variability of the separate ocean and atmosphere results in destruction of the relationship between each northward heat flux component and the respective large-scale latitudinal temperature gradients.

**Acknowledgements** This work was conducted at the Woods Hole Oceanographic Institution's Summer Study Program in Geophysical Fluid Dynamics, which is supported by the National Science Foundation and the Office of Naval Research. Additional funding was provided by the Spanish Ministry of Education (BG), the Department of Energy and the National Science Foundation (PC). Steve Meacham, Phil Morrison, Michael Shelley, George Veronis and Bill Young are gratefully acknowledged for their valuable advice.

## References

Bjerknes J (1964) Atlantic air-sea interaction. Adv Geophys 10: 1–82

Budyko MI (1969) The effect of solar radiation variations on the climate of the Earth. Tellus 21: 611–619

Cessi P (2000) Thermal feedback on wind-stress as a contributing cause of climate variability. J Clim 13: 232–244

Deser C, Blackmon M (1993) Surface climate variations over the North Atlantic ocean during winter 1900–1989. J Clim 6: 1743–1753

Glass L, Mackey MC (1988) From clocks to chaos, the rhythms of life. Princeton University Press, Princeton, pp xvii + 248

Green JSA (1970) Transfer properties of the large scale eddies and the general circulation of the atmosphere. Q. J R Metearol Soc 96: 157–185

Grötzner A, Latif M, Barnett TP (1998) A decadal climate cycle in the North Atlantic Ocean as simulated by the ECHO coupled GCM. J Clim 11: 831–847

Hoskins BJ, Pearce RP (1983) Large-scale dynamical processes in the atmosphere. Academic Press, New York, pp xvi + 397

Jin F-F (1997) A theory of interdecadal climate variability of the North Pacific ocean-atmosphere system. J Clim 10: 1821–1835
Kushnir Y (1994) Interdecadal variations in North Atlantic sea surface temperature and associated atmospheric conditions. J Clim 7: 141–157
Kushnir Y, Held I (1996) Equilibrium atmospheric response to North Atlantic SST anomalies. J Clim 7: 141–157
Latif M, Barnett TP (1994) Causes of decadal climate variability over the North Pacific and North America. Science 266: 634–637
Latif M, Barnett TP (1996) Decadal climate variability over the North Pacific and North America. Dynamics and predictability. J Clim 9: 2407–2423
Lindzen RS, Farrell B (1977) Some realistic modifications of simple climate models. J Atmos Sci 34: 1487–1501
Mann ME, Park J (1996) Joint spatiotemporal modes of surface temperature and sea level pressure variability in the Northern Hemisphere during the last century. J Clim 9: 2137–2162
Manneville P (1990) Dissipative structures and weak turbulence. Academic Press, New York, pp xvii + 485
Moron V, Vautard R, Ghil M (1998) Trends, interdecadal and interannual oscillations in gloval sea-surface temperatures. Clim Dyn 14: 545–569
Nakamura H, Lin G, Yamagata T (1997) Decadal climate variability in the North Pacific during the recent decades. Bull Am Meteorol Soc 78: 2215–2225
Pavan V, Held IM (1996) The diffusive approximation for eddy fluxes in baroclinically unstable jets. J Atmos Sci 53: 1262–1272
Phillips NA (1963) Geostrophic motion. Revi Geophys 1: 123–176
Plaut G, Ghil M, Vautard R (1995) Interannual and interdecadal variability in 335 years of Central England temperatures. Science 268: 710–713
Rhines PB, Young WR (1982) Homogenization of potential vorticity in planetary gyres. J Fluid Mech 122: 347–367
Stone PH (1972) A simplified radiative-dynamical model for the static stability of rotating atmospheres. J Atmos Sci 29: 405–418
Trenberth KE, Hurrell JW (1994) Decadal atmosphere-ocean variations in the Pacific. Clim Dyn 9: 303–319
Trenberth KE, Solomon A (1994) The global heat balance: heat transports in the atmosphere and ocean. Clim Dyn 10: 107–134
Vallis GK (1980) A zonally averaged general circulation model for climate studies. PhD Thesis, Imperial College of Science and Technology, University of London, UK, pp viii + 193
Vallis GK (1982) A statistical-dynamical climate model with a simple hydrology cycle. Tellus 34: 211–227
Wang X, Stone PH, Marotzke J (1995) Poleward heat transport in a barotropic ocean model. J Phys Oceanogr 25: 256–265
Weng W, Neelin JD (1998) On the role of ocean-atmosphere interaction in midlatitude interdecadal variability. Geophys Res Lett 25: 167–170